Hindawi
Complexity
Volume 2018, Article ID 5817597, 12 pages
https://doi.org/10.1155/2018/5817597

Research Article

On an Optimal Control Applied in MEMS Oscillator with Chaotic Behavior including Fractional Order

Angelo Marcelo Tusset, Frederic Conrad Janzen, Rodrigo Tumolin Rocha, and Jose Manoel Balthazar

Department of Mathematics, Federal Technological University of Paraná (UTFPR), 84016-210 Ponta Grossa, PR, Brazil

Correspondence should be addressed to Angelo Marcelo Tusset; tusset@utfpr.edu.br

Received 9 January 2018; Revised 3 July 2018; Accepted 26 July 2018; Published 6 September 2018

Academic Editor: Sigurdur F. Hafstein

The dynamical analysis and control of a nonlinear MEMS resonator system is considered. Phase diagram, power spectral density (FFT), bifurcation diagram, and the 0-1 test were applied to analyze the influence of the nonlinear stiffness term related to the dynamics of the system. In addition, the dynamical behavior of the system is considered in fractional order. Numerical results showed that the nonlinear stiffness parameter and the order of the fractional order were significant, indicating that the response can be either a chaotic or periodic behavior. In order to bring the system from a chaotic state to a periodic orbit, the optimal linear feedback control (OLFC) is considered. The robustness of the proposed control is tested by a sensitivity analysis to parametric uncertainties.

1. Introduction

Currently, a large number of researches have been performed to report nonlinear dynamic phenomena on MEMS resonators [1] as well as application of control techniques to obtain a desired behavior [2]. The nonlinearities in MEMS include nonlinear springs and damping mechanisms [3], nonlinear resistive, inductive and capacitive circuit elements [4], and nonlinear surface, fluid, and electric and magnetic forces [5]. In [6], the Mathieu–van der Pol–Duffing equation was considered to present a MEMS model, and the authors investigated the dynamics of the system considering both forces parametrically and nonparametrically. In [7], a thermomechanical model of the system was developed and explored to explain and predict the entrainment phenomenon. In [8], the nonlinear dynamics of micromechanical oscillators are experimentally explored, and a model was built to explain why high-order entrainment is seen only in doubly supported beams. By its analysis, it is suggested that the strong amplitude–frequency relationship in doubly supported beams enables hysteresis, wide regions of primary entrainment, and high orders of sub and super harmonic entrainment. In [9], a model for oscillations from the continuum description of the temperature and displacement field is considered. A bifurcation analysis of the model was performed, allowing estimating the threshold power for self-oscillation as a function of geometric and optical constants of the beam.

In the work, the dynamical analysis and control of a nonlinear MEMS system is considered, and the 0-1 test is applied to investigate the nonlinear dynamics of the system in fractional order. In order to suppress the chaotic motion, the optimal linear feedback control (OLFC) control is utilized. The robustness of the proposed control is tested by a sensitivity analysis to parametric uncertainties and for variations in fractional order.

With the presented results, it is expected to contribute with new information on the dynamics of the nonlinear MEMS related to the influence of the fractional order in the dynamics of the system and in the robustness of the OLFC control, which is a control technique successfully used in similar systems, where the order of the fractional derivative is considered unitary [2]. In addition, it contributes with new information that can be useful for the study of the application of other control techniques that may be more robust to variations in the fractional derivative, as the SDRE control or

fuzzy control was successfully used in a similar system with fractional unitary order by [2, 10, 11] and [12], respectively.

The 0-1 test can be applied to any system to identify chaotic dynamics. This test uses the temporal series data to characterize the dynamics of the system, analyzing its spectral and statistical properties based on the asymptotic properties of a Brownian motion [13–16].

The optimal linear feedback control (OLFC) was proposed, and the linear feedback control strategies for nonlinear system were formulated, with asymptotic stability of the closed-loop nonlinear system guaranteeing both stability and optimality by [17]. The proposed theorem explicitly expresses the form of the minimized function and gives enough conditions that allow the use of the linear feedback control for nonlinear systems. Recent published works using the OLFC have shown interest in using the control in MEMS [2, 13, 14, 18], and its robustness to control nonlinear systems has been proven in [19] using a polynomial chaos-based framework.

Although it has a long history, the applications of fractional calculus to physics and engineering are just a recent focus of interest [2]. The authors in [2] showed that the fractional order in a MEMS system may produce a chaotic or periodic attractor.

This paper is organized as follows. In Section 2, the mathematical model for microelectromechanical systems (MEMS) is presented and its dynamical analysis considering the nonlinear stiffness term is carried out. In Section 3, the dynamical behavior of the system in fractional order is considered by applying the 0-1 test. In Section 4, the optimal linear feedback control (OLFC) is proposed and applied, and the robustness of the proposed control is tested by a sensitivity analysis to parametric uncertainties. Finally, the paper is concluded in Section 5.

2. Microelectromechanical System (MEMS)

Figure 1 shows a MEMS oscillator composed of a DC source and an alternating current (AC) with a movable microbeam.

Figure 1 represents a device which consists of two fixed plates and a movable plate between them, at which is applied a voltage $V(t)$ composed of a polarization voltage (DC) V_{p}, an alternating voltage (AC) $V_i \sin(wt)$, d (distance between the plates), x (horizontal movement), and m (front panel mass).

According to [10, 12, 20–22], the mathematical model of a MEMS oscillator with cubic nonlinearity term is represented by Figure 1 and can be written as follows:

$$m\ddot{x} + k_1 x + k_3 x^3 + c\dot{x} = \frac{1}{2}\frac{C_0}{(d-x)^2}\left(V_{\mathrm{p}} + V_i \sin(wt)\right) - \frac{1}{2}\frac{C_0}{(d-x)^2}V_{\mathrm{p}}^2, \tag{1}$$

where the coefficient C_0 denotes the capacitance of the parallel-plate actuator.

According to [20–22], the nonlinear electrostatic terms of (1) can be expanded up to the third order based on the Taylor series expansion method, which is represented by the following equation:

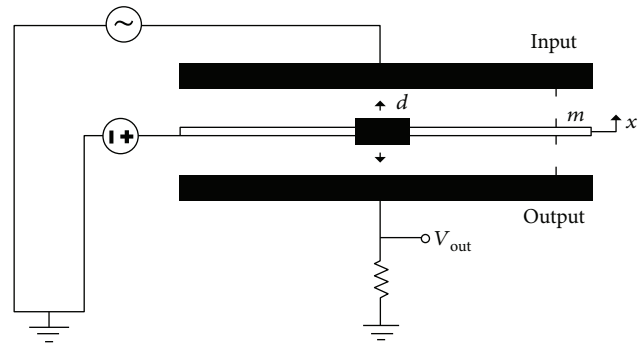

Figure 1: Oscillator microelectromechanical (MEMS).

$$\ddot{x} = -\mu\dot{x} - k_l x - k_{nl}x^3 + \alpha\left(1 + 2x + 3x^2 + 4x^3\right)\sin(wt), \tag{2}$$

where $\mu = c/m$, $k_l = k_1/m$, $k_{nl} = k_3/m$, $\gamma = C_0 \mathrm{V}_{\mathrm{p}}^2/2md^2$, and $\alpha = 2\gamma V_i/V_p$.

Considering $x(0) = x_0$ and $\dot{x}(0) = \dot{x}_0$, and defining the new variables $\tau = wt$ and $u = x/x_0$, (1) can be represented in dimensionless form, denoted by

$$\ddot{u} = -a\dot{u} - bu - cu^3 + d\left(1 + eu + fu^2 + gu^3\right)\sin(\tau), \tag{3}$$

where $a = \mu/w$, $b = k_l/w^2$, $c = k_{nl}x_0^2/w^2$, $d = \alpha/w^2 x_0$, $e = 2x_0$, $f = 3x_0^2$, and $g = 4x_0^3$.

Rewriting (3) in state-space notation, the equations of motion of the system pass to be

$$\begin{aligned}\dot{u}_1 &= u_2,\\ \dot{u}_2 &= -au_2 - bu_1 - cu_1^3 + d\left(1 + eu_1 + fu_1^2 + gu_1^3\right)\sin(\tau),\end{aligned} \tag{4}$$

where $u_1 = u$ and $u_2 = \dot{u}$.

Describing the mathematical equations of the MEMS oscillator, the next subsection will show the dynamical analysis of the system considering the variation of the parameter c, which is the nonlinear stiffness term.

2.1. Numerical Simulations to the Nonlinear Stiffness Term. Figure 2(a) shows the variation of the most significant Lyapunov exponent determined by the Jacobian algorithms [23] considering a period of $\tau = 20{,}000$, and the bifurcation diagram is illustrated in Figure 2(b).

Figure 2(a) shows the variation of the most significant Lyapunov exponent, and the bifurcation diagram is illustrated in Figure 2(b). It provides an illustration on how parameter c influences the system dynamics, as well as for parameters $x_1(0) = 0.0001$, $x_2(0) = 0.0006$, $\alpha = 0.64$, $\mu = 0.03$, $k_l = -0.352$, $\alpha = 0.64$, and $w = 1$ and initial conditions $u_1(0) = 0.0001$ and $u_2(0) = 0.0006$.

As shown in Figure 2, depending on values of "c", the oscillations of (4) can present periodic or chaotic behaviors.

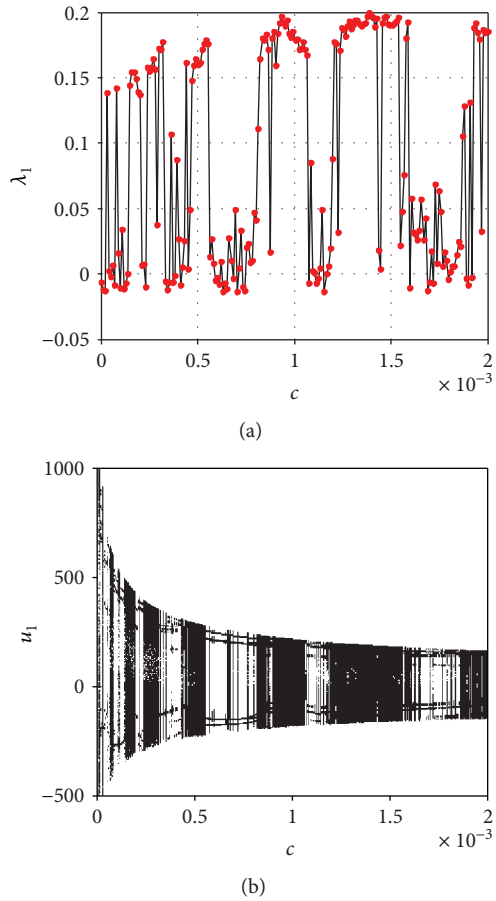

FIGURE 2: (a) Largest Lyapunov exponent for the variation of c and (b) bifurcation diagram for the variation of c.

Figure 3 shows the behavior of (4) for parameter $c = 0.001387$.

Figures 3(a)–3(d) show the time history of displacements of u_1 and u_2, phase plane, and Poincaré map of the system. Those results showed that states u_1 and u_2 support a nonperiodic response of the examined system. Figures 3(e) and 3(d) show the power spectral density (FFT) and the Lyapunov exponent analysis. The frequency spectrum and Lyapunov exponent show that the system stays in a chaotic state for a chosen $c = 0.001387$ parameter.

In the next section, those same analyses will be carried out by considering the fractional order of the system.

3. Chaos in the System with Fractional Order

In this section, the techniques of fractional calculus to analyze the behavior of the system (4) with a fractional order are used. For this behavior, the application of the 0-1 test will be considered in the variable u_1.

The 0-1 test is very useful in fractional-order differential systems. The 0-1 test has been successfully used in the analysis of the chaotic regimes of the MEMS [24, 25]. Basically, the 0-1 test consists of estimating a single parameter K. The test considers a system variable x_j, where two new coordinates (p, q) are defined as follows:

$$p(n,\bar{c}) = \sum_{j=0}^{n} x(j)\cos(j\bar{c}),$$
$$q(n,\bar{c}) = \sum_{j=0}^{n} x(j)\sin(j\bar{c}), \tag{5}$$

where $\bar{c} \in (0, \pi)$ is a constant. The mean square displacement of the new variables $p(n,\bar{c})$ and $q(n,\bar{c})$ are given by

$$M(n,c) = \lim_{n\to\infty} \frac{1}{N}\sum_{j=1}^{N}\left[(p(j+n,\bar{c}) - p(j,\bar{c}))^2 + (q(j+n,\bar{c}) - q(j,\bar{c}))^2\right], \tag{6}$$

where $n = 1, 2, \ldots, N$ and, therefore, the parameter K_c is obtained in the limit for a very long time [15, 16, 24, 25]:

$$K_c = \frac{\operatorname{cov}(Y, M(\bar{c}))}{\sqrt{\operatorname{var}(Y)\operatorname{var}(M(\bar{c}))}}, \tag{7}$$

where $M(\bar{c}) = [M(1,\bar{c}), M(2,\bar{c}), \ldots, M(n_{\max},\bar{c})]$ and $Y = [1, 2, \ldots, n_{\max}]$.

Given any two vectors x and y, the covariance $\operatorname{cov}(x, y)$ and variance $\operatorname{var}(x)$ of $n_{\max}$ elements are usually defined as [15, 16, 24, 25]

$$\operatorname{cov}(x,y) = \frac{1}{n_{\max}}\sum_{n=1}^{n_{\max}}(x(n) - \bar{x})(y(n) - \bar{y}),$$
$$\operatorname{var}(x) = \operatorname{cov}(x,y), \tag{8}$$

where $\bar{x}$ and $\bar{y}$ are the average of $x(n)$ and $y(n)$, respectively. As a final result, the value of the searched parameter K is obtained taking the median of 100 different values of the parameter K_c in (6). If the K value is close to 0, the system is periodic; on the other hand, if the K value is close to 1, the system is chaotic. In all simulations, it has chosen $n = 10000$ and $j = n/100, \ldots, n/10$.

Now, the next subsection will show the dynamical analysis of the system considering the system in fractional order.

3.1. Dynamical Analysis of a Fractional Order. Differential equations may involve Riemann–Liouville differential operators of fractional order $q > 0$, which generally takes the form below [2, 26]

$$D^q x(t) = \frac{1}{\Gamma(m-q)}\int_{t_0}^{t}\frac{x^{(m)}(u)}{(t-u)^{q-m+1}}du, \tag{9}$$

where $m = [q]$, that is, m, is the first integer not less than q. It is easily proved that the definition is the usual derivative definition when $q = 1$. The case $0 < q < 1$ seems to be particularly important; however, there are also some applications for $q > 1$. In this work, for simplicity and without loss of generality, in the following, it is assumed that $t_0 = 0, 0 < q < 1$.

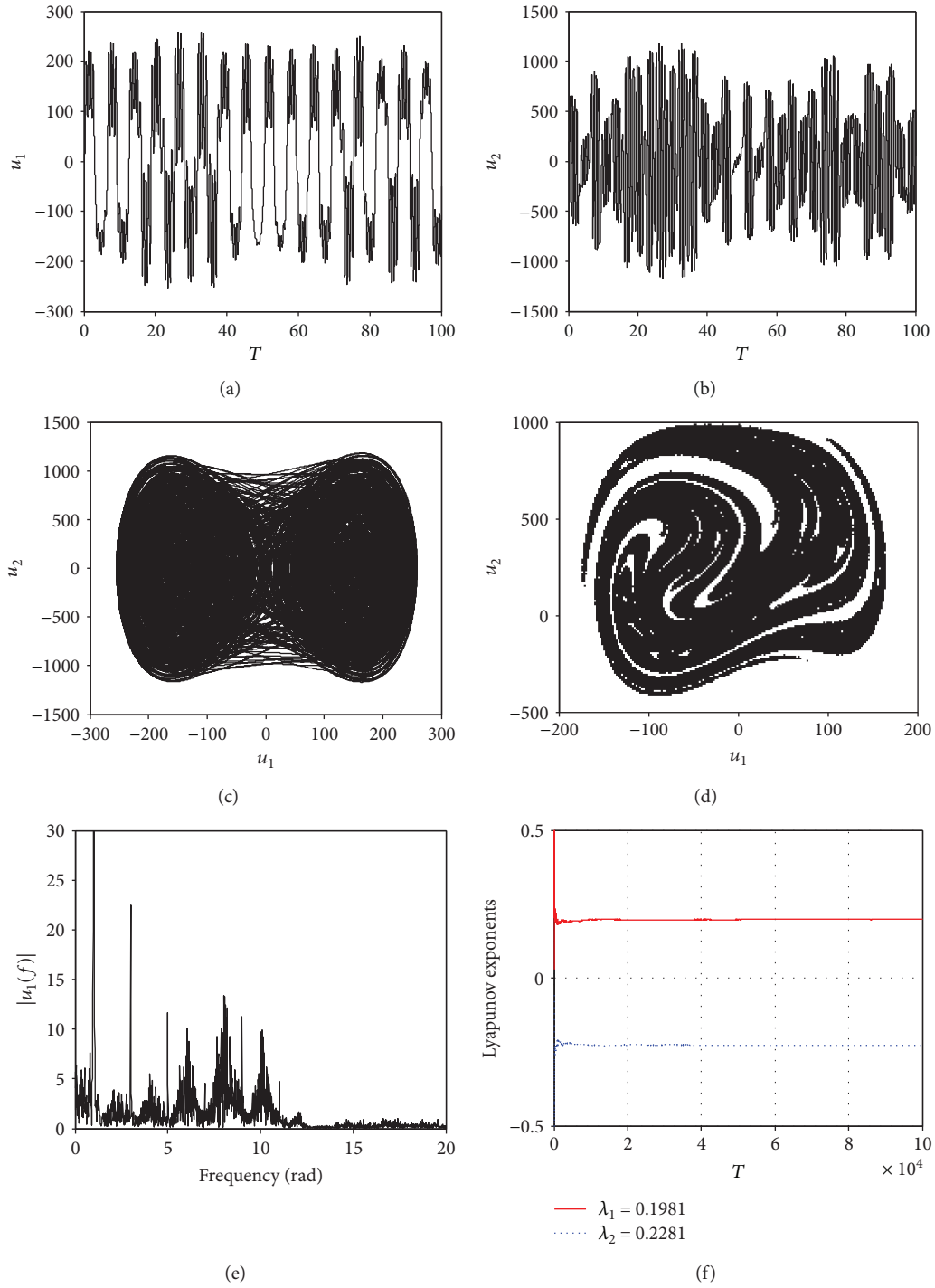

FIGURE 3: (a) Time history of state u_1, (b) time history of state u_2, (c) phase portrait, (d) Poincaré map, (e) power spectral density (FFT) to u_1, and (f) Lyapunov exponents.

The system (4) in fractional order is described as follows:

$$\begin{aligned}\frac{d^{q_1}u_1}{dT^{q_1}} &= u_2,\\ \frac{d^{q_2}u_2}{dT^{q_2}} &= -au_2 - bu_1 - cu_1^3\\ &\quad + d\left(1 + eu_1 + fu_1^2 + gu_1^3\right)\sin(\tau),\end{aligned} \tag{10}$$

where $0 < q_1$ and $q_2 \leq 1$, and its order is denoted by $q = (q_1, q_2)$ here.

The behaviors in fractional order are studied by numerical tools as time histories and phase portraits considering the algorithm proposed by [27].

In Figure 4, the results of the phase portrait are observed, and in Figure 5 is shown the power spectral density (FFT) considering $q_1 = 1$ and $0.4 \leq q_2 \leq 1$.

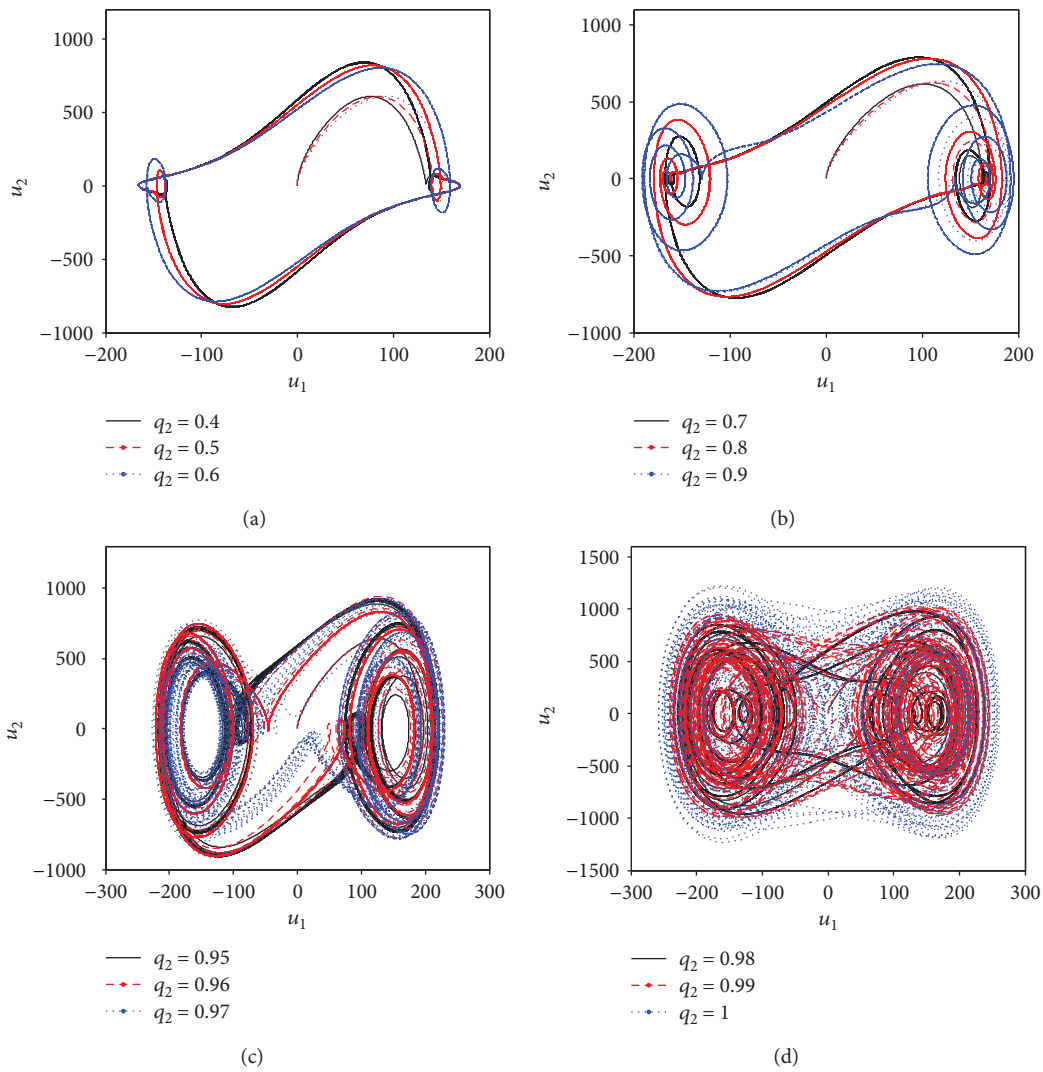

FIGURE 4: MEM system in fractional order. (a) Phase portrait for $q_2 = 0.4$, $q_2 = 0.5$, and $q_2 = 0.6$. (b) Phase portrait for $q_2 = 0.7$, $q_2 = 0.8$, and $q_2 = 0.9$. (c) Phase portrait for $q_2 = 0.95$, $q_2 = 0.96$, and $q_2 = 0.97$. (d) Phase portrait for $q_2 = 0.98$, $q_2 = 0.99$, and $q_2 = 1$.

Analyzing the phase diagrams of Figure 4, it can be observed that the system has periodic behavior for $0.4 \leq q_2 \leq 0.9$ and tends to a quasi-periodic or chaotic behavior for $q_2 > 0.9$. Figure 5 shows the power spectral density (FFT) for the cases observed in Figure 4.

Analyzing the FFT of Figure 5, it is observed that for $0.4 \leq q_2 \leq 0.9$, there is no significant difference between the dominant frequencies. There is only significant difference when $q_2 > 0.9$, being the most significant for $q_2 \geq 0.97$ indicating a chaotic behavior.

To confirm whether the behavior is chaotic or periodic, the 0-1 test is carried out. Figure 6 shows the variation of the value of K of the 0-1 test for the values of q_2 considered in Figures 4 and 5.

The results presented in Figure 6 confirm the behaviors observed in Figures 4 and 5, and the system tends to a chaotic behavior for $q_2 > 0.95$, where $k = 0.901$ for $q_2 = 0.95$, $k = 0.9321$ for $q_2 = 0.96$, $k = 0.9166$ for $q_2 = 0.97$, $k = 0.9392$ for $q_2 = 0.98$, $k = 1$ for $q_2 = 0.99$, and $k = 0.99$ for $q_2 = 0.1$.

The results show that the order of the derivative of q_2 influences the behavior of the system, being that for $q_2 < 0.95$ the system tends to a periodic behavior and for $q_2 > 0.95$ the system tends to be chaotic.

As the chaotic behavior was demonstrated due to the fractional order, the next section will show and design a proposed control to control the chaotic motion.

4. Control Using the Optimal Linear Feedback Control

In order to avoid the chaotic behavior in the system, the optimal linear feedback control is proposed. The objective is to find the optimal control, such that the response of the controlled system (4) results in a periodic orbit $u^*(t)$

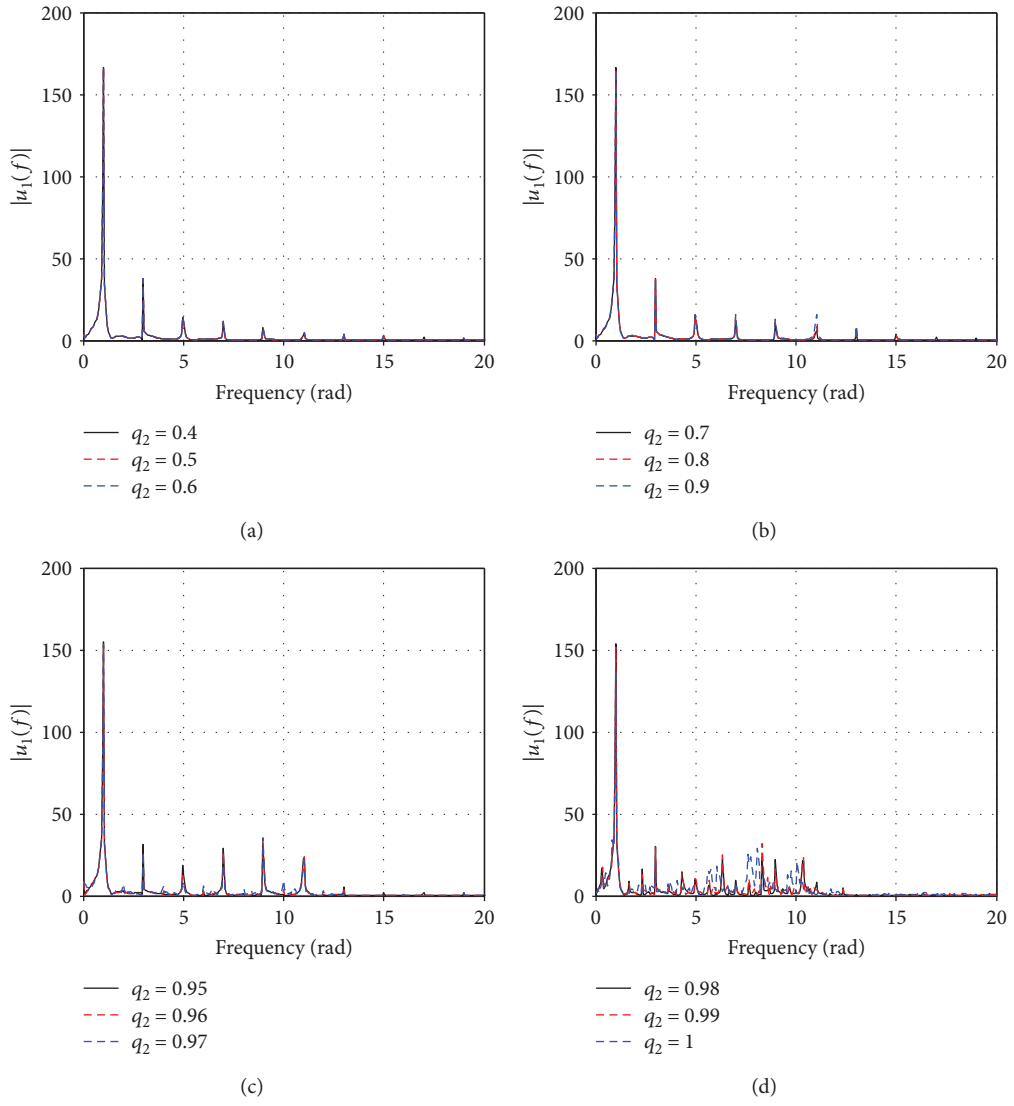

Figure 5: MEM system in fractional order. (a) Power spectral density (FFT) for $q_2 = 0.4$, $q_2 = 0.5$, and $q_2 = 0.6$. (b) Power spectral density (FFT) for $q_2 = 0.7$, $q_2 = 0.8$, and $q_2 = 0.9$. (c) Power spectral density (FFT) for $q_2 = 0.95$, $q_2 = 0.96$, and $q_2 = 0.97$. (d) Power spectral density (FFT) for $q_2 = 0.98$, $q_2 = 0.99$, and $q_2 = 1$.

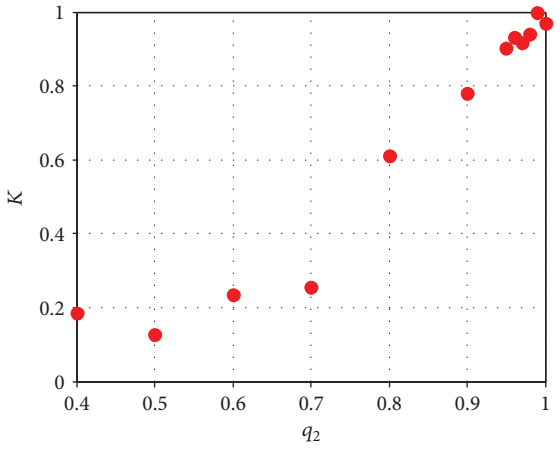

Figure 6: Variations of the 0-1 test for $q_2 = 0.4$, $q_2 = 0.5$, $q_2 = 0.6$, $q_2 = 0.7$, $q_2 = 0.8$, $q_2 = 0.9$, $q_2 = 0.95$, $q_2 = 0.96$, $q_2 = 0.97$, $q_2 = 0.98$, $q_2 = 0.99$, and $q_2 = 1$.

asymptotically stable. Considering the introduction of the control signal U in system (4),

$$\begin{aligned} \dot{u}_1 &= u_2, \\ \dot{u}_2 &= -au_2 - bu_1 - cu_1^3 + d\left(1 + eu_1 + fu_1^2 + gu_1^3\right) \sin(\tau) + U, \end{aligned} \tag{11}$$

where $U = u_r + \tilde{u}$, u_r is the state feedback control, and $\tilde{u}$ is the feedforward control. The control that maintains the system in the desired trajectory is given by

$$\tilde{u} = \dot{u}_2^* + au_2^* + bu_1^* + cu_1^{*^3} - d\left(1 + eu_1^* + fu_1^{*^2} + gu_1^{*^3}\right) \sin(\tau). \tag{12}$$

Substituting (12) in (11) and defining the desired trajectory errors lead to

$$\begin{bmatrix} u_1 \\ u_2 \end{bmatrix} = \begin{bmatrix} u_1 - u_1^* \\ u_2 - u_2^* \end{bmatrix}. \tag{13}$$

System (11) can be represented as deviations in the following way:

$$\begin{aligned} \dot{e}_1 &= e_2, \\ \dot{e}_2 &= -ae_2 - be_1 - c\left((e_1 + u_1^*)^3 - u_1^{*3}\right) \\ &\quad + d\left(1 + ee_1 + f\left((e_1 + u_1^*)^2 - u_1^{*2}\right)\right. \\ &\quad \left. + g\left((e_1 + u_1^*)^3 - u_1^{*3}\right)\right) \sin(\tau) + u_r. \end{aligned} \tag{14}$$

System (14) can be represented in the deviation as

$$\dot{e} = Ae + G(e, u^*) + Bu_r, \tag{15}$$

or in matrix form

$$\begin{bmatrix} \dot{e}_1 \\ \dot{e}_2 \end{bmatrix} = \begin{bmatrix} 0 & 1 \\ -a & -b \end{bmatrix} \begin{bmatrix} e_1 \\ e_2 \end{bmatrix} + G(e, u^*) + \begin{bmatrix} 0 \\ 1 \end{bmatrix} u_r, \tag{16}$$

where

$$G(e, u^*) = \begin{bmatrix} 0 \\ -c\left((e_1 + u_1^*)^3 - u_1^{*3}\right) + d\left(1 + ee_1 + f\left((e_1 + u_1^*)^2 - u_1^{*2}\right) + g\left((e_1 + u_1^*)^3 - u_1^{*3}\right)\right) \sin(\tau) \end{bmatrix}. \tag{17}$$

According to [2], for matrices Q and R, positive definite symmetric matrices, the control u_r is optimal and transfers the nonlinear system (14) from any initial state to the final state $e(\infty) = 0$.

Minimizing the functional obtains

$$J = \int_0^\infty \left(e^T Qe + u_r^T Ru_r\right) dt. \tag{18}$$

The control u_r can be found by solving the equation

$$u_r = -R^{-1}B^T Pe = -K_r e. \tag{19}$$

P is the symmetric matrix and can be found from the algebraic Riccati equation

$$PA + A^T P - PBR^{-1}B^T P + Q = 0. \tag{20}$$

Matrices A and B of system (16) are represented by

$$\begin{aligned} A &= \begin{bmatrix} 0 & 1 \\ -a & -b \end{bmatrix}, \\ B &= \begin{bmatrix} 0 \\ 1 \end{bmatrix}. \end{aligned} \tag{21}$$

Defining Q and R matrices obtains

$$\begin{aligned} Q &= \begin{bmatrix} 100 & 50 \\ 50 & 100 \end{bmatrix}, \\ R &= [1]. \end{aligned} \tag{22}$$

The system of (20) can be solved, obtaining

$$\begin{aligned} p &= \begin{bmatrix} 59.9500 & 10.3582 \\ 10.3582 & 59.9500 \end{bmatrix}, \\ K_r &= [\,10.3582 \quad 10.9571\,]. \end{aligned} \tag{23}$$

Substituting K_r in (19), the control signal is obtained as

$$\begin{aligned} u_r &= -10.3582e_1 - 10.9571e_2 \\ &= -10.3582(u_1 - u^*{}_1) - 10.9571(u_2 + u^*{}_2). \end{aligned} \tag{24}$$

First of all, it is important to define the desired trajectory $u^*(t)$, which will be considered as $u^*{}_1 = 258 \sin(\tau)$ and $u^*{}_2 = 258 \cos(\tau)$, whose amplitudes are near the maximum amplitude of displacement of u_1 observed in Figure 2(a) and the predominant frequency observed in Figure 2(f).

The time history of displacement of the controlled system can be observed in Figure 7(a), and the phase portrait is shown in Figure 7(b), desired trajectory errors in Figure 7(c), and signal control in Figure 7(d), considering the application of the control U in (11).

As can be seen in Figure 7, the OLFC control was efficient with null error for $\tau > 1.5$ (Figure 3(c)), considering the maximum error in a permanent state of 2% and that the linear feedback u_r control is only used to bring the system to the desired orbit and that the feedforward ($\tilde{u}$) control maintains the system in the desired orbit (Figure 7(d)).

Next, the same proposed control is applied considering parametric errors.

4.1. Proposed Control with Parametric Errors. In order to determine the effects of uncertainties on the performance of the controller, it is estimated that an error of ±20% is encountered in parameters a, b, c, d, f, and g, with a similar strategy

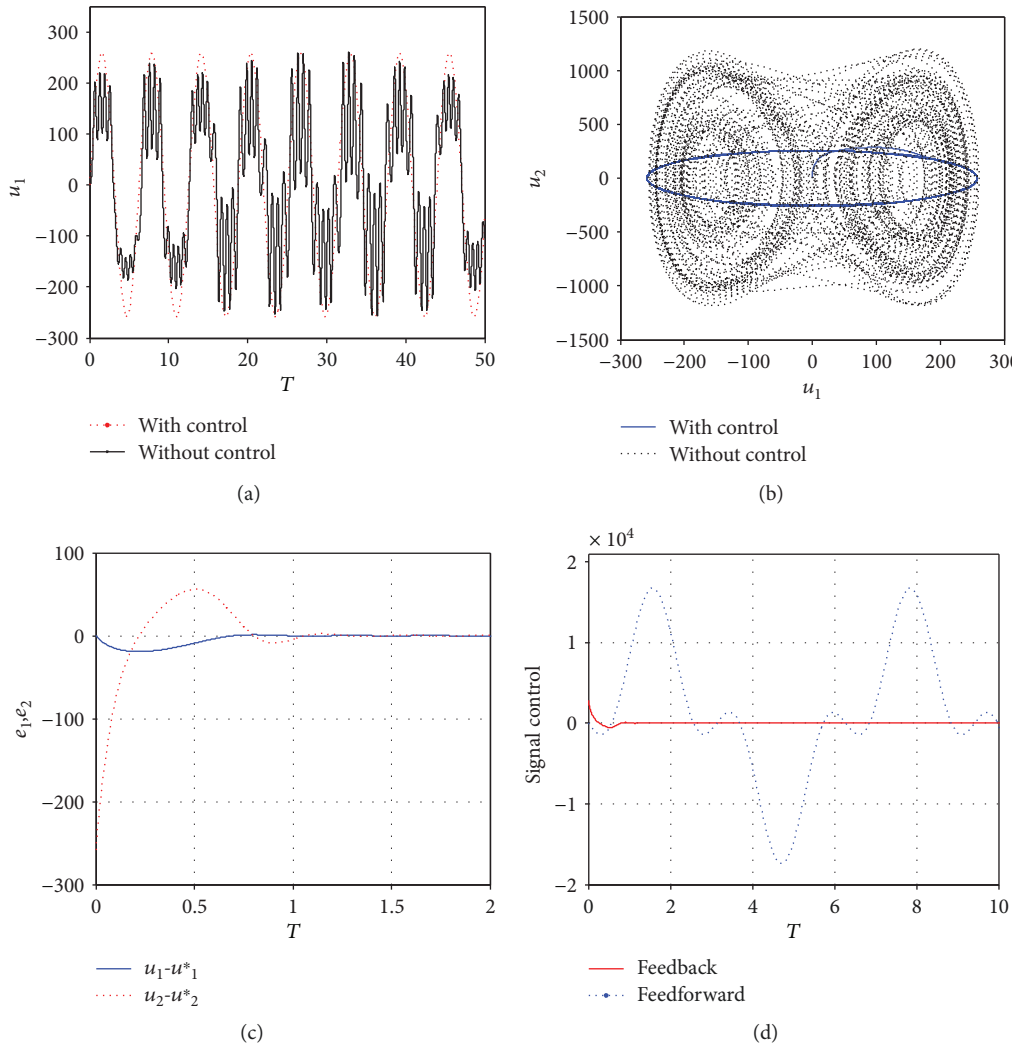

FIGURE 7: MEM system with proposed control. (a) Time history of state u_1, (b) phase portrait, (c) desired trajectory errors, and (d) signal control.

used in [10, 14, 28]. In addition, the variation of the fractional derivative q_2 in the robustness of the proposed control will be considered.

In Figures 8, 9, and 10, the robustness of the control to maintain the system in a periodic orbit is observed, considering the proposed control with variation in parameters $a_u = a(0.8 + 0.4r(t))$, $b_u = b(0.8 + 0.4r(t))$, $c_u = c(0.8 + 0.4r(t))$, $d_u = d(0.8 + 0.4r(t))e_u = e(0.8 + 0.4r(t))$, $f_u = f(0.8 + 0.4r(t))$, and $g_u = g(0.8 + 0.4r(t))$, where $r(t)$ is a random number $r(t) = [0, 1]$. In Figure 11, the robustness of the control to maintain the system in a periodic orbit is observed considering the proposed control with parameters $q_2 = 0.4$, $q_2 = 0.5$, $q_2 = 0.7$, $q_2 = 0.9$, $q_2 = 0.98$, and $q_2 = 0.99$.

Considering that $e_{-c} = [\,|u_{1c} - u^u_{1c}| \quad |u_{2c} - u^u_{2c}|\,]^T$ and u_{-c} are the states obtained with the control without parametric uncertainties and u^u_{-c} is the state obtained with the control with parametric uncertainties, in Figure 8 the robustness of the control can be observed in keeping the system in the same orbit obtained with the control without uncertainties, considering the uncertainties only in the feedback control (u_r), with the matrix $A = \begin{bmatrix} 0 & 1 \\ -a_u & -b_u \end{bmatrix}$.

As can be seen in Figure 8, even with uncertainties in the feedback control, the control was robust with an absolute maximum error of approximately $|e_{1c}| \approx 0.0395$ and $|e_{2c}| \approx 0.894$.

In Figure 9, it is possible to observe the robustness of the control in keeping the system in the same orbit obtained with the control without uncertainties, considering the uncertainties only in the feedforward control ($\tilde{u}$), with the feedforward control in form $\tilde{u} = \dot{u}^*_2 + a_u u^*_2 + b_u u^*_1 + c_u u^{*^3}_1 - d_u(1 + e_u u^*_1 + f_u u^{*^2}_1 + g_u u^{*^3}_1) \sin(\tau)$.

As can be seen in Figure 9, even with uncertainties in the feedforward control, the control was robust with an absolute maximum error of approximately $|e_{1c}| \approx 5.264$ and $|e_{2c}| \approx 50.56$.

In Figure 10, the robustness of the control in keeping the system in the same orbit obtained with the control without

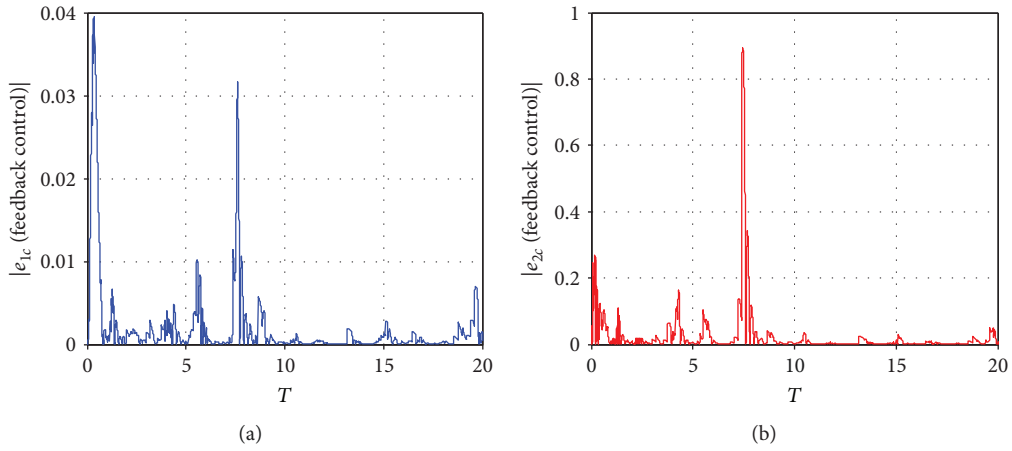

Figure 8: Deviation of the desired trajectory with the proposed control with parametric errors in feedback control u: (a) deviation of the desired trajectory $e_{1c} = |u_{1c} - u^u_{1c}|$ and (b) deviation of the desired trajectory $e_{2c} = |u_{2c} - u^u_{2c}|$.

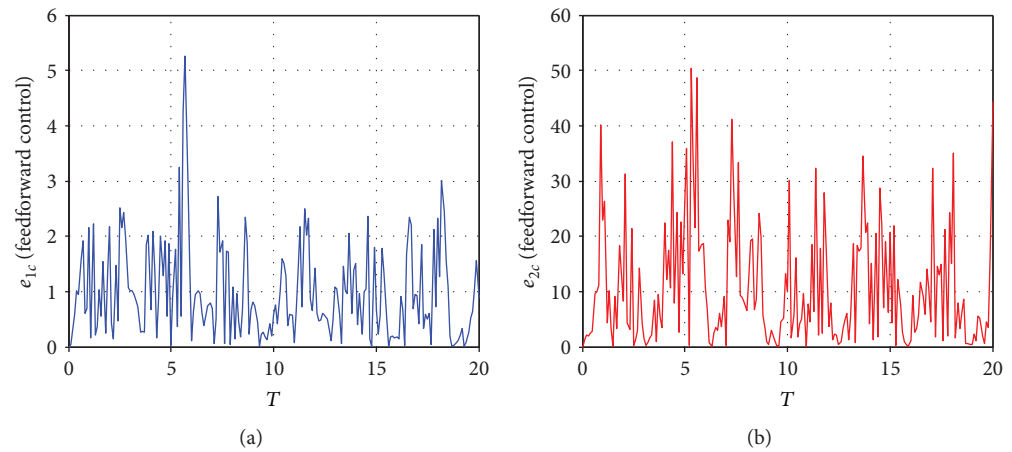

Figure 9: Deviation of the desired trajectory with the proposed control with parametric errors in feedforward control ($\tilde{u}$): (a) deviation of the desired trajectory $e_{1c} = |u_{1c} - u^u_{1c}|$ and (b) deviation of the desired trajectory $e_{2c} = |u_{2c} - u^u_{2c}|$.

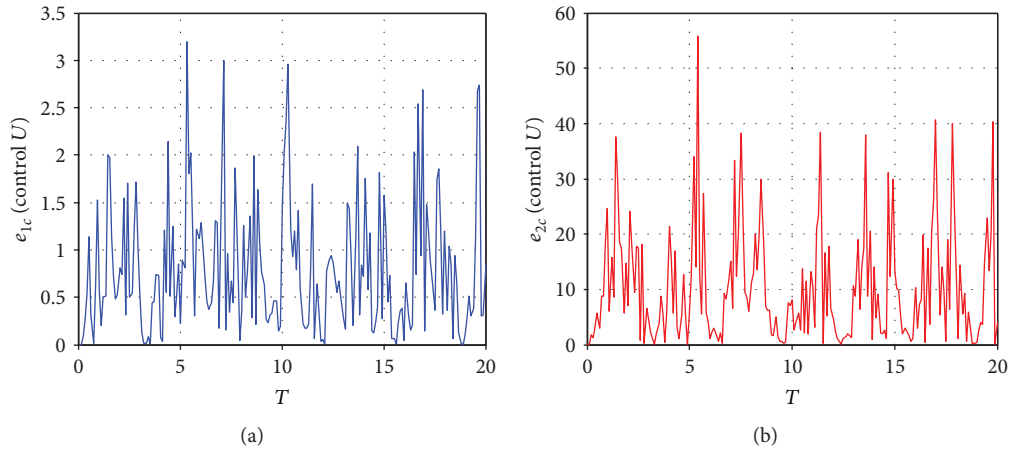

Figure 10: Deviation of the desired trajectory with the proposed control with parametric errors in feedback control and feedforward: (a) deviation of the desired trajectory $e_{1c} = |x_{1c} - x^u_{1c}|$ and (b) deviation of the desired trajectory $e_{2c} = |x_{2c} - x^u_{2c}|$.

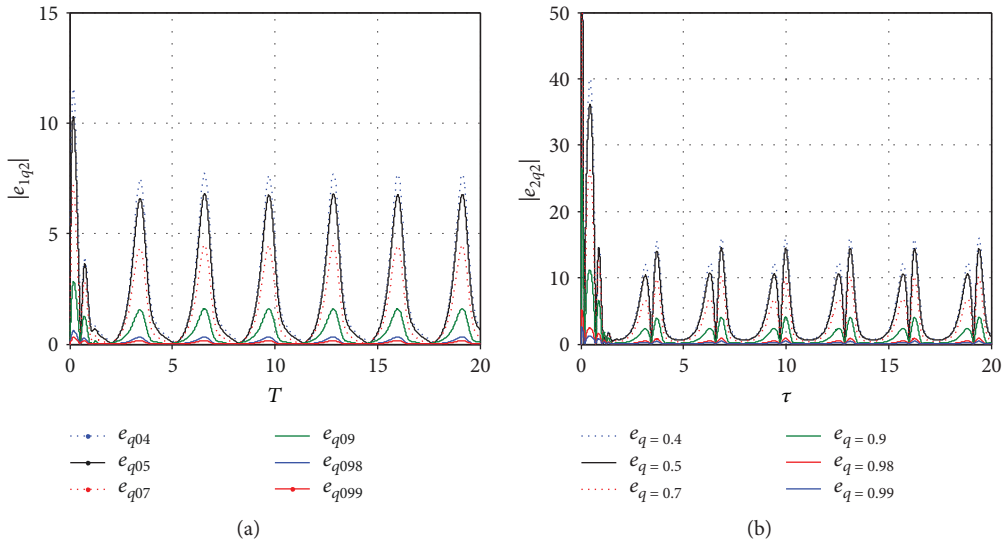

FIGURE 11: Deviation of the desired trajectory with the proposed control for variations in $q_2 = 0.4$, $q_2 = 0.5$, $q_2 = 0.7$, $q_2 = 0.9$, $q_2 = 0.98$, and $q_2 = 0.99$. (a) Deviation of the desired trajectory $e_{1q2} = |u_{1q2} - u^u_{1q2}|$ and (b) deviation of the desired trajectory $e_{2q2} = |u_{2q2} - u^u_{1q2}|$.

uncertainties is observed, considering the uncertainties in feedback control (u_r) and in the feedforward control ($\tilde{u}$), with the feedforward control in the form $\tilde{u} = \dot{u}^*_2 + a_u u^*_2 + b_u u^*_1 + c_u u^{*^3}_1 - d_u(1 + e_u u^*_1 + f_u u^{*^2}_1 + g_u u^{*^3}_1) \sin(\tau)$ and the matrix $A = \begin{bmatrix} 0 & 1 \\ -a_u & -b_u \end{bmatrix}$.

As can be seen in Figure 10, even with uncertainties in the feedforward control, the control was robust with an absolute maximum error of approximately $|e_{c1}| \approx 3.192$ and $|e_{c2}| \approx 55.84$.

In Figure 11, the robustness of the control in keeping the system in the same orbit obtained with the control with $q_2 = 1$ can be observed. It is considered that $e_{-q2} = \left[\, |u_{1q2} - u^u_{1q2}| \; |u_{2q2} - u^u_{1q2}| \,\right]^T$ and u_{-q2} are the states obtained with the control with $q_2 = 1$ and u^u_{-q2} is the state obtained with the control with $q_2 \neq 1$.

As can be observed in Figure 11, the error increases when $u_1 \to 0$ and $u_2 \to 0$ and $q_2 < 1$, indicating that the control is sensitive to variations in q_2.

In Figure 12, the error considering the maximum amplitudes of oscillation of the system with control is observed. In this case, it is considered that $e_{mq2u-} = \left[\, |u_{mq2u1} - u^u_{mq2u1}| \; |u_{mq2u2} - u^u_{mq2u2}| \,\right]^T$ and u_{mq2u-} are the maximum amplitudes of oscillation obtained with the control with $q_2 = 1$ and u^u_{mq2u-} is the maximum amplitude of oscillation obtained with the control with $q_2 \neq 1$.

As can be seen in Figure 12, the control with variations in q_2 has smaller errors at the peak points than when it is close to zero, thus keeping the displacement amplitudes close to those desired, even with variations in q_2, demonstrating that for control applications of cases very different from $q_2 = 1$, it is necessary to design a new control feedforward control that considers the fractional derivatives and new values of Q and R for the feedback control.

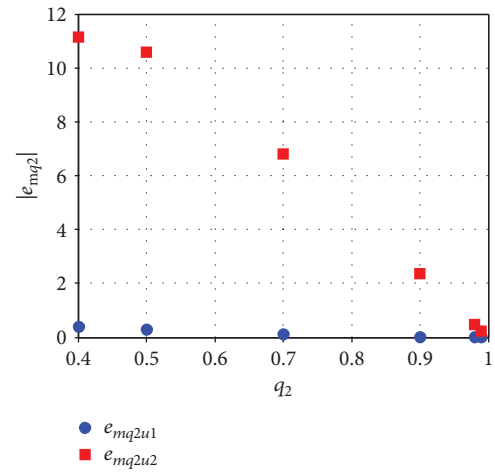

FIGURE 12: Deviation of the desired maximum amplitudes of oscillation with the proposed control for variations in $q_2 = 0.4$, $q_2 = 0.5$, $q_2 = 0.7$, $q_2 = 0.9$, $q_2 = 0.98$, and $q_2 = 0.99$. (a) Deviation of the desired maximum amplitudes of oscillation $e_{1q2} = |u_{1q2} - u^u_{1q2}|$ and (b) deviation of the desired maximum amplitudes of oscillation $e_{2q2} = |u_{2q2} - u^u_{2q2}|$.

5. Conclusions

This work investigated the dynamical behavior of a MEMS system in fractional order. The numerical simulations showed the existence of chaotic behavior for some regions in the parameter space of the fractional order and regions in the parameter of the nonlinear stiffness term; this behavior was characterized by the 0-1 test. The bifurcation diagrams were constructed to explore the qualitative behavior of the system.

In order to suppress such chaos, the optimal linear feedback control (OLFC) was projected. The efficiency of the technique was demonstrated through numerical simulations

in order to eliminate the chaotic behavior of the system. As can be seen, the strategy was efficient to maintain the amplitude of the oscillator in the desired periodic orbit $u^*_1 = 258 \sin(\tau)$ and $u^*_2 = 258 \cos(\tau)$, and it can be seen that the control is sensible to variations in order of the fractional order.

Thus, it is possible to conclude that the results obtained for the capacitive MEMS oscillator model considered in this work can be considered for other capacitive models with similar formulation, such as the model used by [2, 10], in which the OLFC control was successfully used even to parametric uncertainties.

The main contribution of this work is the results obtained by considering the sensitivity control for fractional derivative variation presented in Figures 11 and 12, because there are some results that were not observed in previous works, then demonstrating the importance of the controller design taking into account the order of the fractional derivative, which is related to the effects of memory of the material, such as the behavior observed in viscoelastic materials or with similar behavior. It can also be observed that the error increases as the derivative (q_2) moves away from the derivative $q_2 = 1$, which is the value of the derivative normally used in the control design.

With those results, it is intended for a future work to perform the analysis of the robustness of other control techniques for the capacitive MEMS oscillator model, as well as to verify if it is possible to improve the robustness of the OLFC control for variations of the fractional order.

Data Availability

The data used to support the findings of this study are available from the corresponding author upon request.

Conflicts of Interest

The authors declare that there is no conflict of interest regarding the publication of this paper.

Acknowledgments

The authors acknowledge support by CNPq (Grant 447539/2014-0) and CAPES, all Brazilian research funding agencies.

References

[1] R. M. C. Mestrom, R. H. B. Fey, J. T. M. Van Beek, K. L. Phan, and H. Nijmeijer, "Modelling the dynamics of a MEMS resonator: simulations and experiments," *Sensors and Actuators A: Physical*, vol. 142, no. 1, pp. 306–315, 2008.

[2] A. M. Tusset, J. M. Balthazar, D. G. Bassinello, B. R. Pontes, and J. L. P. Felix, "Statements on chaos control designs, including a fractional order dynamical system, applied to a "MEMS" comb-drive actuator," *Nonlinear Dynamics*, vol. 69, no. 4, pp. 1837–1857, 2012.

[3] M. Roukes, "Nanoelectromechanical systems face the future," *Physics World*, vol. 14, no. 2, pp. 25–32, 2001.

[4] H. Xie and G. K. Fedder, "Vertical comb-finger capacitive actuation and sensing for CMOS-MEMS," *Sensors and Actuators A: Physical*, vol. 95, no. 2-3, pp. 212–221, 2002.

[5] M. I. Younis and A. H. Nayfeh, "A study of the nonlinear response of a resonant microbeam to an electric actuation," *Nonlinear Dynamics*, vol. 31, no. 1, pp. 91–117, 2003.

[6] M. Pandey, R. H. Rand, and A. T. Zehnder, "Frequency locking in a forced Mathieu–van der Pol–Duffing system," *Nonlinear Dynamics*, vol. 54, no. 1-2, pp. 3–12, 2008.

[7] K. Aubin, M. Zalalutdinov, T. Alan et al., "Limit cycle oscillations in CW laser-driven NEMS," *Journal of Microelectromechanical Systems*, vol. 13, no. 6, pp. 1018–1026, 2004.

[8] D. B. Blocher, A. T. Zehnder, and R. H. Rand, "Entrainment of micromechanical limit cycle oscillators in the presence of frequency instability," *Journal of Microelectromechanical Systems*, vol. 22, no. 4, pp. 835–845, 2013.

[9] D. Blocher, R. H. Rand, and A. T. Zehnder, "Analysis of laser power threshold for self oscillation in thermo-optically excited doubly supported MEMS beams," *International Journal of Non-Linear Mechanics*, vol. 57, pp. 10–15, 2013.

[10] A. M. Tusset, Á. M. Bueno, C. B. Nascimento, M. dos Santos Kaster, and J. M. Balthazar, "Nonlinear state estimation and control for chaos suppression in MEMS resonator," *Shock and Vibration*, vol. 20, no. 4, 761 pages, 2013.

[11] N. J. Peruzzi, F. R. Chavarette, J. M. Balthazar, A. M. Tusset, A. L. P. M. Perticarrari, and R. M. F. L. Brasil, "The dynamic behavior of a parametrically excited time-periodic MEMS taking into account parametric errors," *Journal of Vibration and Control*, vol. 22, no. 20, pp. 4101–4110, 2016.

[12] H. S. Haghighi and A. H. D. Markazi, "Chaos prediction and control in MEMS resonators," *Communications in Nonlinear Science and Numerical Simulation*, vol. 15, no. 10, pp. 3091–3099, 2010.

[13] G. A. Gottwald and I. Melbourne, "A new test for chaos in deterministic systems," *Proceedings of the Royal Society A: Mathematical, Physical and Engineering Sciences*, vol. 460, no. 2042, pp. 603–611, 2004.

[14] G. A. Gottwald and I. Melbourne, "Testing for chaos in deterministic systems with noise," *Physica D: Nonlinear Phenomena*, vol. 212, no. 1-2, pp. 100–110, 2005.

[15] D. Bernardini and G. Litak, "An overview of 0-1 test for chaos," *Journal of the Brazilian Society of Mechanical Sciences and Engineering*, vol. 38, no. 5, pp. 1433–1450, 2016.

[16] A. M. Tusset, F. C. Janzen, V. Piccirillo, R. T. Rocha, J. M. Balthazar, and G. Litak, "On nonlinear dynamics of a parametrically excited pendulum using both active control and passive rotational (MR) damper," *Journal of Vibration and Control*, vol. 24, no. 9, pp. 1587–1599, 2017.

[17] M. Rafikov and J. M. Balthazar, "On an optimal control design for Rössler system," *Physics Letters A*, vol. 333, no. 3-4, pp. 241–245, 2004.

[18] F. R. Chavarette, J. M. Balthazar, J. L. P. Felix, and M. Rafikov, "A reducing of a chaotic movement to a periodic orbit, of a micro-electro-mechanical system, by using an optimal linear control design," *Communications in Nonlinear Science and Numerical Simulation*, vol. 14, no. 5, pp. 1844–1853, 2009.

[19] M. d. F. V. Pereira, J. M. Balthazar, D. A. dos Santos, A. M. Tusset, D. F. de Castro, and I. A. A. Prado, "A note on polynomial chaos expansions for designing a linear feedback control for nonlinear systems," *Nonlinear Dynamics*, vol. 87, no. 3, pp. 1653–1666, 2017.

[20] S. Sabarathinam and K. Thamilmaran, "Implementation of analog circuit and study of chaotic dynamics in a generalized Duffing-type MEMS resonator," *Nonlinear Dynamics*, vol. 87, no. 4, pp. 2345–2356, 2017.

[21] E. M. Miandoab, H. N. Pishkenari, A. Yousefi-Koma, and F. Tajaddodianfar, "Chaos prediction in MEMS-NEMS resonators," *International Journal of Engineering Science*, vol. 82, pp. 74–83, 2014.

[22] E. M. Miandoab, A. Yousefi-Koma, H. N. Pishkenari, and F. Tajaddodianfar, "Study of nonlinear dynamics and chaos in MEMS/NEMS resonators," *Communications in Nonlinear Science and Numerical Simulation*, vol. 22, no. 1-3, pp. 611–622, 2015.

[23] A. Wolf, J. B. Swift, H. L. Swinney, and J. A. Vastano, "Determining Lyapunov exponents from a time series," *Physica D: Nonlinear Phenomena*, vol. 16, no. 3, pp. 285–317, 1985.

[24] D. G. Bassinello, J. M. Balthazar, A. M. Tusset, and V. Piccirillo, "Dynamic analysis of a fractional-order MEMS system using 0-1 test," in *ASME 2016 International Design Engineering Technical Conferences and Computers and Information in Engineering Conference*, p. 9, Charlotte, NC, USA, August 2016.

[25] A. M. Tusset, J. M. Balthazar, J. J. de Lima, R. T. Rocha, F. C. Janzen, and P. S. Yamaguchi, "On an optimal control applied in atomic force microscopy (AFM) including fractional-order," in *ASME 2017 International Design Engineering Technical Conferences and Computers and Information in Engineering Conference*, p. 9, Cleveland, OH, USA, August 2017.

[26] Y. Yu, H. X. Li, S. Wang, and J. Yu, "Dynamic analysis of a fractional-order Lorenz chaotic system," *Chaos, Solitons & Fractals*, vol. 42, no. 2, pp. 1181–1189, 2009.

[27] I. Petráš, *Fractional-Order Nonlinear Systems: Modeling, Analysis and Simulation*, Nonlinear Physical Science, Springer Science & Business Media, 2011.

[28] J. M. Balthazar, D. G. Bassinello, A. M. Tusset, A. M. Bueno, and B. R. de Pontes Junior, "Nonlinear control in an electromechanical transducer with chaotic behaviour," *Meccanica*, vol. 49, no. 8, pp. 1859–1867, 2014.